Deactivation of phosphorus-poisoned Pd/SSZ-13 for the passive adsorption of NOx

Downloaded from: https://research.chalmers.se, 2024-03-20 10:57 UTC

Citation for the original published paper (version of record):
Feizie Ilmasani, R., Yao, D., Ho, H. et al (2022). Deactivation of phosphorus-poisoned Pd/SSZ-13 for the passive adsorption of NOx. Journal of Environmental Chemical Engineering, 10(3). http://dx.doi.org/10.1016/j.jece.2022.107608

N.B. When citing this work, cite the original published paper.

research.chalmers.se offers the possibility of retrieving research publications produced at Chalmers University of Technology. It covers all kind of research output: articles, dissertations, conference papers, reports etc. since 2004. research.chalmers.se is administrated and maintained by Chalmers Library

(article starts on next page)

Journal of Environmental Chemical Engineering 10 (2022) 107608

Contents lists available at ScienceDirect

Journal of Environmental Chemical Engineering

journal homepage: www.elsevier.com/locate/jece

Deactivation of phosphorus-poisoned Pd/SSZ-13 for the passive adsorption of NO_x

Rojin Feizie Ilmasani, Dawei Yao, Phuoc Hoang Ho, Diana Bernin, Derek Creaser, Louise Olsson *

Chemical Engineering, Competence Center for Catalysis, Chalmers University of Technology, Gothenburg SE-412 96, Sweden

ARTICLE INFO

Editor: Dong-Yeun Koh

Keywords:
Cold start
PNA
Palladium zeolite
Phosphorus poisoning
Catalyst deactivation

ABSTRACT

Automotive catalysts can be exposed to various poisonous substances that can cause physical or chemical deactivation. One of such poisons is phosphorous, which originates from lubricant oils. This study focuses on the phosphorus deactivation of Pd/SSZ-13 used as a passive NO_x adsorber (PNA). A clear deactivation caused by phosphorus was observed, and it was increased by increasing the content of phosphorous. It was concluded that phosphorous can cause both physical and chemical deactivation. This was evident from XPS analysis, where the presence of phosphorus pentoxide (P_2O_5) causes physical deactivation whereas metaphosphate (PO_3^-) and phosphate (PO_4^{3-}) cause chemical deactivation. Also, it was shown that metaphosphates (PO_3^-) become the dominant phosphorous species at higher P concentrations. Lesser amounts of O_2 were released in P-poisoned Pd/SSZ-13, as was found in oxygen TPD when increasing the P concentration, due to the presence of more PO_3^- species. Furthermore, XRD and ^{27}Al NMR analyses revealed that phosphorus also interacted with alumina in the zeolite framework by forming Al-O-P species; this was also supported by SEM-EDX, where there was a clear overlap of P with Al and Pd spectra. DRIFTS analysis showed that OH groups in contact with the zeolite structure became contaminated by phosphorus and caused a chemical deactivation of Pd/SSZ-13. It was also found that, during multiple cycles, the PNA capacity decreased for phosphorus-poisoned samples. This was caused by the transformation of P_2O_5, which causes physical blocking, to PO_3^-, which interacts chemically with the palladium species.

1. Introduction

The abatement of NO_x has been one of the main challenges facing exhaust after-treatment systems (EATS) in lean-burn combustion engines. The two technologies used most often for reducing NO_x are Lean NO_x trapping (LNT) and selective catalytic reduction (SCR) [1–5]. However, they both suffer from kinetic limitations with respect to deNO_x performance at low exhaust temperatures (< 200 °C) [6–8]. A possible solution here is to use a passive NO_x adsorber (PNA) prior to the SCR catalyst to capture NO_x at low temperatures and release it gradually at higher temperatures (> 200 °C), which allows the SCR catalyst to convert it by reaction with NH_3. Several potential adsorbents have been studied for the PNA process by employing different noble metal catalysts, such as Pd, Pt and Ag on high surface area supports [9,10]. In one study by Crocker et al., a significant increase in NO_x adsorption was seen at low temperatures when Pt and Pd on CeO_2-ZrO_2 were used in the PNA processes [11]. Moreover, Ag/Al_2O_3 was found to be a capable NO_x adsorbent at low temperatures, although small quantities of hydrogen were also required [12]. These materials can nevertheless be vulnerable to SO_2, which is inevitably present in exhaust gases [13,14]. Ma et al. on the other hand, established a dynamic equilibrium on CeO_2 by sulphate formation and decomposition, which reduced the deactivation effect of SO_2 in NH_3-SCR systems. Interestingly, the addition of small MnO_x clusters to the CeO_2 improved the SCR performance and kept the strong resistance to SO_2 poisoning [15]. Ryou et al. reported high adsorption ability of Pd/CeO_2 due to presence of Pd, however, sulphur aging treatment caused the deactivation of this sample since the presence of SO_2 reduced the interaction of PdO and CeO_2 which led to lower NO adsorption [13]. Consequently, new studies on the zeolite supports BEA, CHA and MFI have therefore been conducted using mainly Pd as the noble metal [14,16,17]. Zheng et al. studied different Pd-supported zeolite adsorbents in PNA processes, focusing on the effect of Pd

* Corresponding author.
E-mail address: louise.olsson@chalmers.se (L. Olsson).

https://doi.org/10.1016/j.jece.2022.107608
Received 14 November 2021; Received in revised form 16 March 2022; Accepted 21 March 2022
Available online 24 March 2022
2213-3437/© 2022 The Author(s). Published by Elsevier Ltd. This is an open access article under the CC BY license (http://creativecommons.org/licenses/by/4.0/).

dispersion [17]. They found that different Pd species are involved in NO_x adsorption, including Pd^{2+} and Pd^{4+}; it was suggested that, in the presence of water in the inlet gas, the main adsorption is related to Pd^{2+} sites [17]. In another study, Ryou et al. found that hydrothermal aging at 750 ℃ caused PdO species to transform into Pd^{2+}, which lead to an increase in the NO_x adsorption of Pd/SSZ-13 [18].

Vu et al. investigated the positive effect of adding a small amount of CO, which resulted in increases in both NO_x adsorption and the desorption temperature [19]. However, some recent studies have reported a large deactivation of Pd/zeolites due to the presence of high concentrations of CO in multiple NO storage and release cycles [20–22]. Another common deactivation process that exhaust after-treatment catalysts are subjected to is chemical poisoning from the fuel or components in the engine's lubricant oils. Zinc dialkyldithiophosphate (ZDDP), a common lubricant oil, contains phosphorus that can deactivate the catalyst [23,24]. It is known that its high stability makes deactivation by phosphorus one of the most severe and causes difficulty in regenerating catalysts [24,25]. Phosphorus poisoning has been investigated in several studies of SCR and DOC catalysts [23,26–28]. Toops et al., who studied the P-poisoning of $Pt/CeO_2/Al_2O_3$, reported the formation of aluminium phosphate in the front of the DOC [24]. Wang et al. discovered that phosphorus poisoned both the active sites and the OH groups in $Pd\text{-}Pt/Al_2O_3$ [29]. We investigated the phosphorus deactivation of Cu/SSZ-13 used for SCR in an earlier study and found that metaphosphates were the main phosphorus compound in the sample [26]. Moreover, hydrothermal aging of the phosphorus-poisoned samples resulted in the formation of $AlPO_4$, which lead to destruction of the support [30,31]. In a very recent study from Chen et al. on phosphorous poisoning of Pd/zeolite in PNA processes, formation of metaphosphates were confirmed as a dominant P compound [32].

In this study, the deactivation of Pd/SSZ-13 caused by phosphorus poisoning was investigated for the PNA processes, with focus being placed on the effect of the content of phosphorus and the changes of the poisoning effect during multiple cycles. The deactivation was studied using a flow reactor for the adsorption and desorption of NO_x. The PNAs were characterised using BET surface area, ICP-SEMS, O_2-TPD, SEM-EDX mapping, XRD, XPS, NMR and in situ DRIFT spectroscopy to obtain an improved understanding of the physical and chemical effects phosphorus has on Pd/SSZ-13.

2. Experimental

2.1. Catalyst synthesis and phosphorous poisoning

SSZ-13 was synthesised using a hydrothermal method [3] thus: 0.8 g NaOH (Sigma-Aldrich, > 98%) was dissolved in 66 g MilliQ water before about 18 g SDA (TMAda-OH, Sigma-Aldrich) and 1.38 g $Al(OH)_3$ (Sigma-Aldrich) were added to the solution under stirring. Then, 12 g of fumed silica (Sigma-Aldrich, average particle size 7 nm) was gradually added to the mixture; to achieve a fully homogenised gel, while vigorous stirring was applied. The prepared mixture was transferred to a Teflon-lined autoclave, stirred and heated continuously at 160 ℃ for 96 h. Thereafter, the autoclaves were cooled to ambient temperature and the slurry was washed 10 times with MilliQ water until a pH < 8 was reached. The separated solid was dried overnight at 85 ℃ before being calcined at 600 ℃ for 8 h. The ion-exchange procedure was carried out twice, using 43.2 g of NH_4NO_3 (Sigma-Aldrich, 99%) and 100 ml MilliQ water at 80 ℃ for 15 h, to produce NH_4/SSZ-13 [3]. This step was followed by drying the powder overnight at 85 ℃ and calcination at 550 ℃ for 4 h. A solution of $Pd(NO_3)_2$ was used for 1 wt% Pd loading on the zeolite support using an incipient wetness impregnation method; the retrieved powder was dried overnight at 85 ℃ and then calcined at 500 ℃ for 5 h in air.

Ryou et al. observed an increased NO_x adsorption for Pd/SSZ-13 after hydrothermal aging at 750 ℃ due to the transformation of PdO species to Pd^{2+} [18]. Therefore, in our study, the Pd/SSZ-13 was first degreened at 750 ℃ using 400 ppm NO. 8% O_2 and 5% H_2O for 1 h by placing the Pd/SSZ-13 powder in a crucible in the flow reactor (see Section 2.3). The phosphorous was then impregnated on the adsorbent, using the incipient wetness impregnation, with an aqueous $(NH_4)_2HPO_4$ solution. This was followed by drying overnight prior to calcination at 550 ℃ for 4 h. Phosphorus was applied on the adsorbents in three different concentrations, namely 0.4, 0.6 and 0.8 mmol g^{-1}, with the two higher concentrations being prepared by increasing the phosphorous loading for part of the 0.4 mmol g^{-1} main batch. In this study, the phosphorous (P)-poisoned samples were denoted as 0.4P, 0.6P and 0.8P, respectively and the reference sample (lacking phosphorous) as Pd/SSZ.

Washcoated monoliths were prepared for each adsorbent and used for further adsorption and desorption measurements in the flow reactor. Cordierite monoliths (cpsi 400), 2 cm in length and 2.1 cm in diameter, were used and about 700 mg powder (using 5% boehmite as a binder) was used in each washcoat. All the prepared monoliths were calcined at 500 ℃ for 5 h in air prior to being used in the flow reactor.

2.2. Characterisation techniques

The samples were characterised twice: those treated for 1 h under 400 ppm NO, 8% O_2, 5% H_2O and Ar at 750 ℃ are denoted "degreened" and those that underwent NO temperature programme desorption (TPD) experiments are denoted "reacted". The degreened samples are powder degreened in the flow reactor, while the reacted samples are scraped off washcoats from the used monoliths. However, freshly calcined powder was used for ICP-SFMS and BET measurements. Elemental analysis of all the calcined samples was conducted using ICP-SFMS from ALS Scandinavia AB; the BET surface area was measured using N_2 physisorption in a Tristar 3000 (Micromeritics) device after the samples had been degassed overnight at 220 ℃.

Powder X-ray diffraction (XRD) was performed on both degreened and reacted samples in a SIEMENS diffractometer D5000 that operates with Cu Kα radiation (λ = 1.5418 Å) at 40 kV and 40 mA. The data collection range was between 5° to 45° with a step size of 0.01. X-ray photoelectron spectroscopy (XPS) analysis was conducted using a PHI5000 VersaProbe III system equipped with a monochromatic Al K X-ray source (E = 1486.6 eV). Narrow scan measurements were aligned with the C-C carbon Peak (C1s) with a binding energy of 284.6 eV before analysis. An FEI Quanta 200 Environmental SEM (ESEM) coupled with an Oxford X-max 80 EDX detector was employed for SEM images and EDX mapping. Transmission electron microscopy images were collected for degreened samples by using a FEI Titan 80-300 TEM. The samples were pestled using an agate mortar and then placed on the porous carbon films with the support of copper grids. Solid-state ^{27} Al NMR spectra were gathered for both degreened and reacted samples on a Bruker Avance III 500 MHZ spectrometer utilising a 4 mm double-resonance MAS probe; the rotor was spun at 5000 Hz. A single pulse experiment (hpdec) was used with an ^{1}H decoupling (SPINAL64) of about 83 kHz. Normalisation of the spectra was conducted by weight and the number of scans accumulated. A moderate function was applied to the free induction decays prior to Fourier transformation.

A powder flow reactor equipped with mass flow controllers for gas feed and a Hiden HPR-20 QUI mass spectrometer (MS) was used in the oxygen TPD experiments. For both degreened and reacted samples, approx. 50 mg of powder was loaded in the quartz tube. In this experiment, 3% O_2/Ar at a flow of 20 ml/min was used. The oxygen adsorption step was at 25 ℃ for 5 min, followed by heating up to 400 ℃ under the same gas conditions and then maintaining this temperature for 30 min. After cooling to ambient temperature, 1 h of Ar flush was performed followed by increasing the temperature to 800 ℃, at a rate of 20 ℃/min, in the presence of Ar alone.

Diffuse Reflectance Infra-red Fourier Transformed Spectroscopy (DRIFTS) was used to examine the surface species. The degreened samples were placed on a porous grid in a reaction cell equipped with CaF_2 windows and pretreated with 8% O_2, 1% H_2O and Ar at 550 ℃ for

Table 1
Elemental analysis, BET surface area and pore volume of the calcined and poisoned samples.

Sample	Pd (wt%)	P (wt%)	S_{BET} (m^2g^{-1})	V_{pore} (g/cm^3)
Pd/SSZ	1.1	–	602.7	0.28
Pd/SSZ-0.4P	1.0	1.3	562.3	0.26
Pd/SSZ-0.6P	1.04	1.5	535.1	0.25
Pd/SSZ-0.8P	1.1	2.6	519.5	0.24

15 min. Two NO TPD cycles were conducted, with an adsorption step at 80 ℃, using 200 ppm NO, 1% H_2O and 8% O_2 for 15 min, followed by a desorption step at 550 ℃ under the same gas mixture conditions. The samples were subsequently treated with 200 ppm NO, 400 ppm CO, 1% H_2O and 8% O_2 in Ar for 15 min using the same desorption procedure as in the first cycle. Prior to each adsorption, a pre-treatment step at 550 ℃ with 8% O_2, 1% H_2O and Ar for 15 min was applied and the spectra were collected during the adsorption steps.

2.3. Adsorbent activity measurements

It is of great importance to PNA studies that the steps of both adsorption and desorption of NO_x species are examined. In this study, these steps were carried out in a flow reactor: this setup is discussed in more detail in our previous paper [33]. In brief, the coated monoliths were placed in a quartz tube and a heating coil wound around it was used to heat up the reactor. The temperatures of the adsorbent and the gases were measured by two thermocouples and the outlet gases by a MKS Multi-Gas 2030 HS FTIR. A total flow of 550 Nml min^{-1} was used in the NO TPD experiments, using Ar as a balance gas at atmospheric pressure. A degreening step was conducted at 750 ℃ with 400 ppm NO, 8% O_2, 5% H_2O and Ar for a period of 1 h for the calcined Pd/SSZ-13 monolith. In the case of the P-poisoned samples, the degreening step was carried out on the catalyst powder before the phosphorous was loaded because high temperature treatment of phosphorus-poisoned samples could alter the poisoning or result in severe aging, as was found in our earlier study of P-poisoned Cu/SSZ-13 [34]. The NO temperature programme desorption (TPD) experiments were performed with an adsorption step at 80 ℃ using 200 ppm NO, 8% O_2, 5% H_2O and Ar for 2 h. This was followed by flushing the catalyst with 8% O_2, 5% H_2O for 20 min and thereafter increasing the temperature to 550 ℃, at a rate of 20 ℃/min, in the same gas mixture. Finally, the temperature was maintained at 550 ℃ for 30 min. Four additional NO-TPD cycles were conducted with different parameters: TPD 2, where the NO concentration was changed; TPD 3, where the total flow was changed; TPD 4, where the NO concentration was changed; and TPD 5, which was the same as TPD 1. The so-called "reacted sample" refers to the powder scraped from the monolith that had run all 5 cycles. Moreover, the "degreened sample" is related to the powder after the degreening step at 750 ℃ for both poisoned and non-poisoned samples. Since the focus of this study is the effect phosphorus has on a PNA procedure we have concentrated on the results of TPD 1, which we also compared with TPD 5 to examine the changes that occurred after multiple cycles.

3. Results and discussions

3.1. Characterisation of P-poisoned catalysts

The amounts of palladium and phosphorous present were determined using ICP-SFMS; the results are reported in Table 1. The H-SSZ-13 had a Si/Al ratio of 11.5 and the Na content of the prepared H-SSZ-13 was < 0.05 wt%, which has been found to be beneficial for the hydrothermal stability and catalyst activity of the Cu/SSZ-13 used for NH_3 SCR [35,36]. The results in the table also show that there was no effect on the content of Pd after the addition of phosphorous; this was also observed by Xie et al. after loading P on Cu-SSZ-13 [37]. The intended phosphorus contents of 0.4, 0.6 and 0.8 mmol g^{-1}, resulted in 1.3, 1.5 and 2.6 wt%, respectively, which were very close to the theoretical values. The specific surface area and the pore volume of the fresh and P-poisoned samples were examined by nitrogen physisorption, the results of which are given in Table 1. As expected, both the surface area and pore volume of the P-poisoned samples decreased when the phosphorous contents in the adsorbents increased. This indicates that phosphorous impregnation had a physical effect, i.e. pore blockage of the Pd/SSZ-13: an effect that was intensified when the concentration of P was increased.

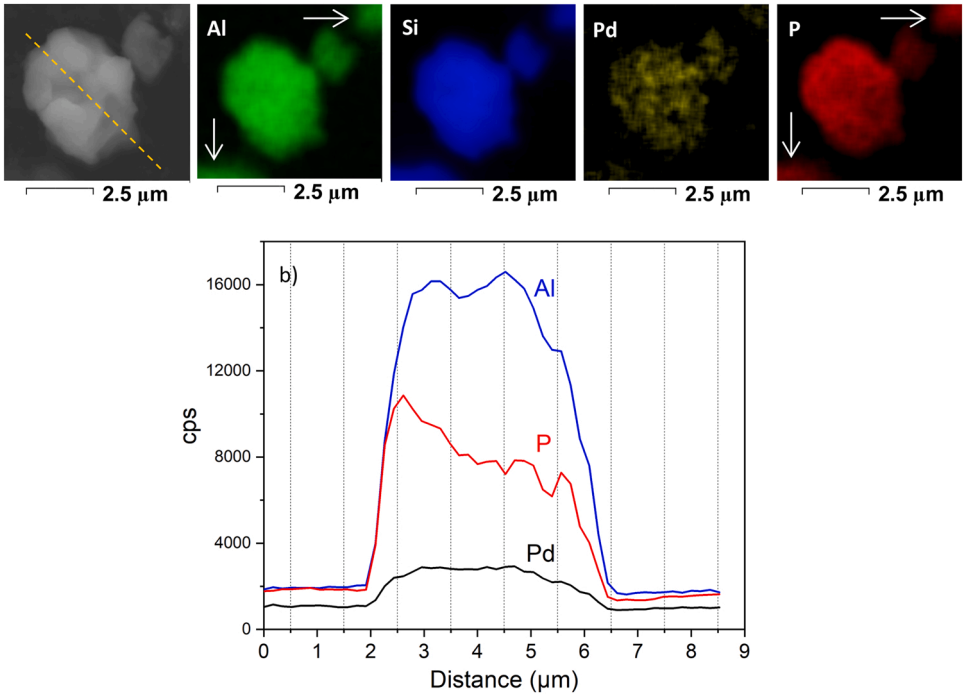

Fig. 1. a) SEM-EDX mapping of Pd/SSZ-0.4P; b) EDX line scan profiles for Pd, P and Al (according to the dashed line shown in the leftmost image in Fig. a).

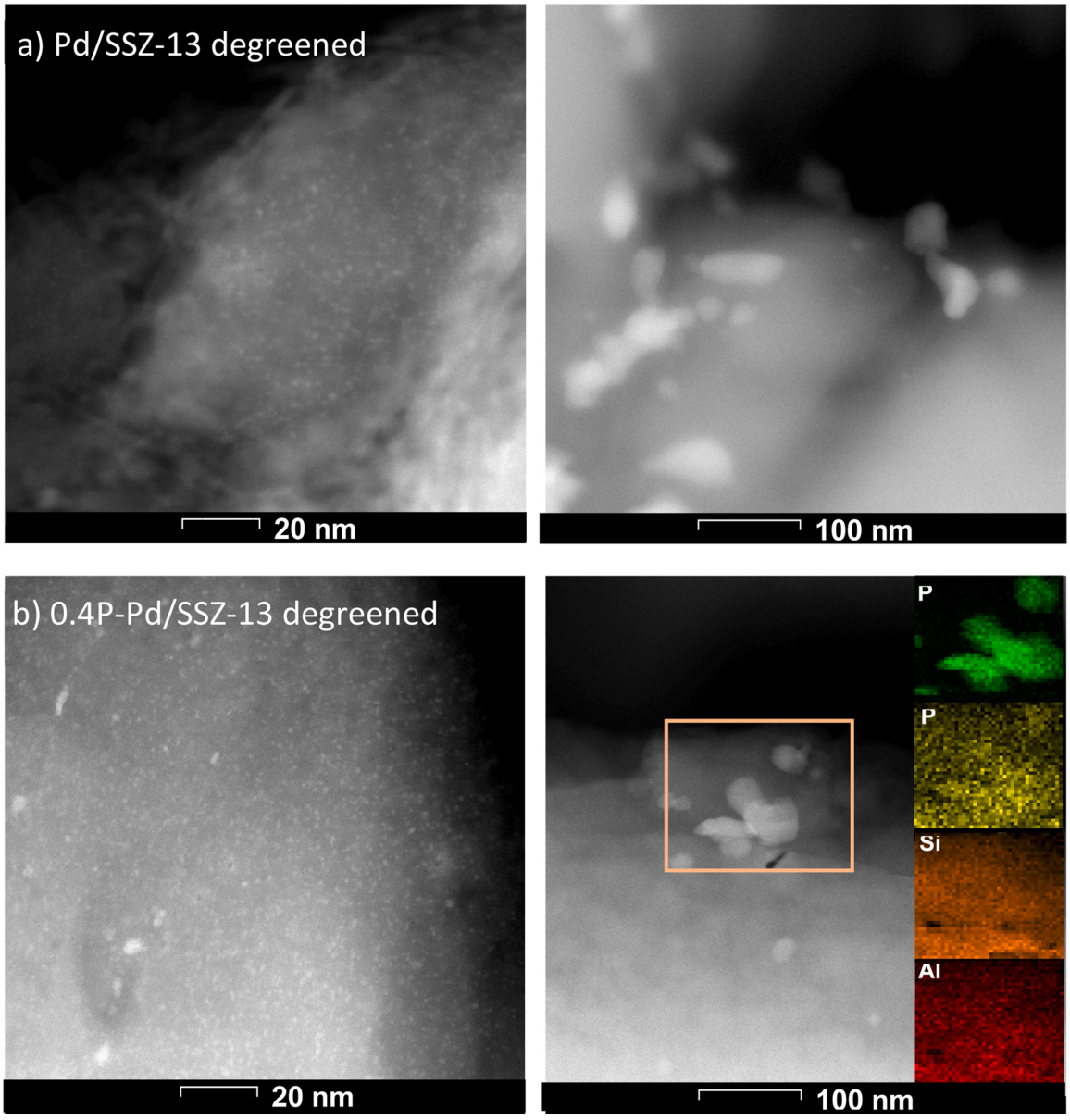

Fig. 2. TEM images of degreened a) Pd/SSZ-13 and b) 0.4P-Pd/SSZ-13 samples within two scales of 20 and 100 nm.

SEM-EDX elemental mapping was conducted to study the distribution of Al, Si, P and Pd in the 0.4 P-poisoned sample and the results obtained are shown in Fig. 1. The measurements were made using a scale of 2.5 μm. Fig. 1a indicates a uniform distribution for both Al and Si. Pd mapping was weaker than the other components due to the low concentration of palladium. However, mappings of both P and Pd displayed several Pd-rich and P-rich areas where many overlaps were detected between Pd and P which was also detected in TEM-EDX mappings as well (Fig. 2b). Such overlaps were also detected between Al and P (shown by arrows), suggesting the interaction of P with both Pd and the zeolite framework. The line scan profiles (Fig. 1b) obtained for Al, Pd and P also confirm that Al, Pd and P co-exist in the same area. These results are similar to those we found from EDX mapping analysis in our previous study on the phosphorus poisoning of Cu/SSZ-13 [31]. The TEM images in Fig. 2 illustrate an even distribution of Pd particles in both non-poisoned and poisoned samples. In Pd/SSZ-13 sample, small Pd particles were detected with sizes ranging between 3 and 7 nm. In addition, also larger clusters of about 50–100 nm were observed and these were likely formed during palladium impregnation in the synthesis. TEM images for 0.4P-Pd/SSZ-13 also confirmed an even distribution of Pd particles on the surface and no clear effect regarding phosphorous addition on the Pd particle sizes was found.

X-ray diffraction was used to investigate the crystallinity of degreened and P-poisoned samples and the results are illustrated in Fig. 3. The reacted samples were scraped from monoliths after the NO TPD cycles. All the peak positions were normalised to the main zeolite peak at 20.9° in order to provide a clear understanding of the effect that phosphorous has on the structure. As shown in Fig. 3a, the structure of Pd/SSZ-13 was well maintained after the P poisoning: no new peaks were detected that could be assigned to the P species (phosphorus pentoxide, metaphosphate and phosphate), thereby indicating that a high dispersion of phosphorus was attained after impregnation. However, the peaks around $2\theta = 9.6°$, 18° and 25.3° had shifted towards lower degrees after P poisoning (Fig. 3c): a shift can be explained by Bragg's law ($d = n\lambda/2sin\theta$) [38], which suggests an expansion of the lattice planes in the framework. The same shift was observed in our previous studies in the P-poisoning of Cu/SSZ-13, caused by lattice expansion of the zeolite framework [31,34]. We, therefore, suggest that

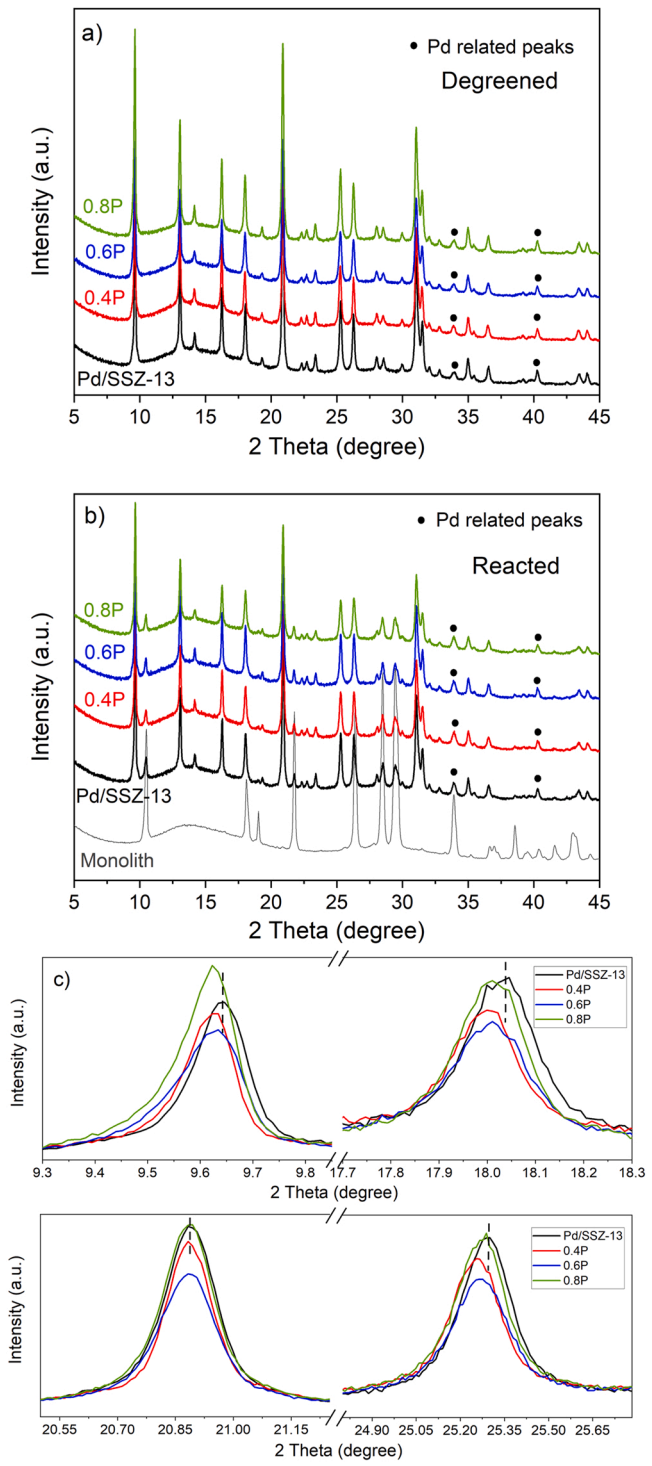

Fig. 3. XRD patterns of the P-poisoned and non-poisoned Pd/SSZ-13. a) degreened samples; b) reacted samples scraped off the monoliths; c) magnification of four areas in Figure (a).

the same applies to this case too, i.e. some of the phosphorus species were probably located inside the zeolite framework and caused this lattice expansion. Furthermore, the palladium peaks that were observed at $2\theta = 33.8°$ and 40.2° are assigned to PdO and Pd, respectively [20,39]. These peaks clearly maintained their position and intensity in the P-poisoned samples, thereby showing that the larger Pd particles were preserved. The peaks in the reacted samples in Fig. 3b show that the structure of the zeolite was well maintained. The PdO peak at $2\theta = 33.8°$ was similar for the degreened and reacted samples (Fig. S1, Supplementary material). The intensity was nevertheless slightly higher for the reacted samples, which can be explained by the fact that these also contain some binder from the coating process. In addition, there is possibly an overlap by a peak related to the monolith in the same area, which could interfere with the results.

Fig. 4 shows the XP spectra of degreened P-poisoned Pd/SSZ-13. The main peaks observed on the surface were related to P 2P, with the intensity of the peak increasing as the loadings of phosphorous increase. A slight shift of the P 2P peak could be noticed towards lower binding energies by increasing the P concentration. Deconvolution was conducted for the phosphorous peaks using three phosphorous species: phosphorus pentoxide (P_2O_5, at ~ 135.6 eV), metaphosphate (PO_3^-, at ~ 134.5 eV) and phosphate (PO_4^{3-} at ~ 133.2 eV) [40,41]. The dominant phosphorus species in the 0.4P sample was phosphorus pentoxide: increasing the P loading to 0.8P, however, caused more metaphosphate species to form and the amount of P_2O_5 decreased. This was also observed in other studies for P-poisoned catalysts, where a high loading of P tended to result in more glassy metaphosphates [30,32,34,42,43]. According to the literature, phosphorous can cause both physical deactivation (by blocking active sites) and chemical deactivation (by interacting with active sites or supports) in the catalyst [30,42,44]. The decreasing trend in the BET surface area, shown in Table 1, indicates that phosphorous masks the surface and blocks the pores of the adsorbents, thereby leading to physical deactivation. XPS analysis can provide more insight into the phosphorus deactivation effect. It is known that phosphoric acid and metaphosphoric acid decompose at low temperatures (around 160–200 °C) [34], so the presence of phosphorus in an acidic form is therefore not to be expected on the catalyst surface. Phosphorous can nevertheless be found in the form of P_2O_5 on the catalyst surface: phosphorus pentoxide is an anhydride form of the acid and can block active sites by creating polycyclic dimers [34]. Furthermore, phosphates can form due to the interaction of P with the catalyst [24,45]. Since XPS analysis shows the presence of both P_2O_5 and PO_3^-/PO_4^{3-} in all loadings of P, it can be concluded that the adsorbents had undergone both physical deactivation (due to the presence of P_2O_5) and chemical (due to the presence of PO_3^-/ PO_4^{3-}).

The elemental analysis from ICP in Table 1 can be used to determine the molar ratio of (PO_3^-+ PO_4^{3-})/Pd in the P-poisoned adsorbents: these were found to be 4, 5 and 8, respectively, for 0.4P, 0.6P and 0.8P. In the case of sample 0.8P, for example, the XPS results given in Fig. 4b show the formation of about 60% of the PO_3^-+ PO_4^{3-} and that results in a molar ratio of (PO_3^-+ PO_4^{3-})/Pd of 4.8. If the ratio would have been < = 1 it would have been possible that the phosphates may only have attached to palladium. However, since the ratio is significantly larger than 1, it indicates that the phosphorous interacts with both the Pd to form Pd(II) metaphosphate and phosphates, as well as forming $AlPO_4$ and/or $Al(PO_3)_3$ through interaction with the zeolite support [24,34].

The P spectra after the reaction (Fig. 5) showed a shift towards binding energies lower than those of the degreened samples (Fig. 4). The results obtained from the deconvolution suggest that this shift is due to the formation of more PO_3^-. It is interesting to note that these results indicate that, during the NO-TPD cycles, a part of the physical deactivation due to P_2O_5 was shifted to chemical deactivation by the transformation of P_2O_5 into PO_3^-. These results could explain why the final cycle of the NO TPD (repetition of the first cycle) for the P-poisoned samples showed a lower adsorption/desorption capacity than the first cycle, and this is discussed in more detail in Section 3.2.

Oxygen temperature programme desorption was performed from 25 to 800 °C to investigate the effect of phosphorus on the oxygen desorption from the Pd species. The oxygen desorption peaks related to poisoned and non-poisoned samples are shown in Fig. 6. Degreened Pd/SSZ-13 had the main desorption peak at 525 °C, which could be assigned to the release of lattice oxygen generated from the decomposition of PdO_x species [46,47]. The P-poisoned samples showed a weaker intensity of this peak and more of a broader range of oxygen release. It should be noted that O_2-TPD was also performed for H-SSZ-13 (not

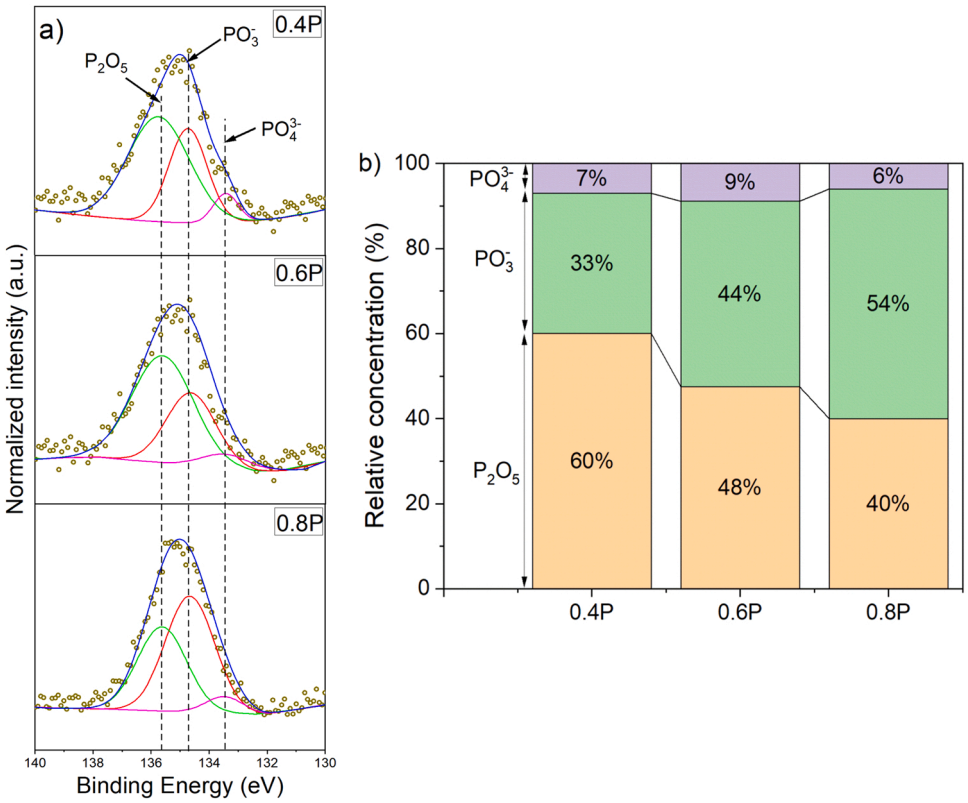

Fig. 4. a) XP P 2p spectra of the 0.4P, 0.6P and 0.8P degreened samples. (b) The corresponding relative concentrations of the three phosphorus compounds obtained from spectral deconvolution.

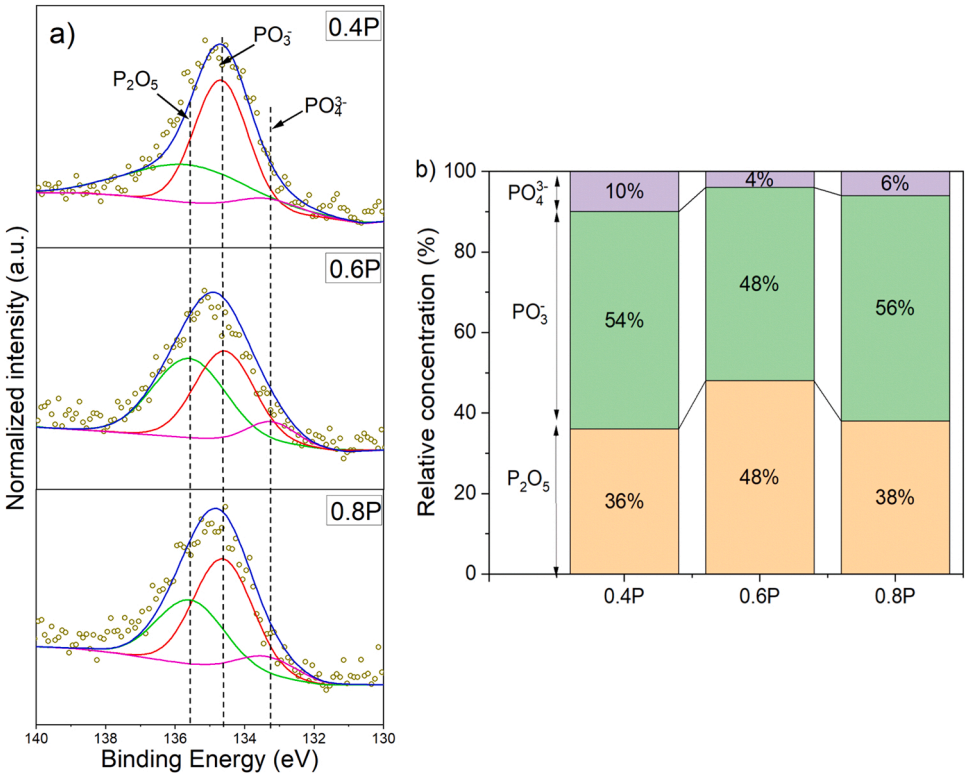

Fig. 5. a) XP P 2p spectra of the 0.4P, 0.6P and 0.8P reacted samples. (b) The corresponding relative concentrations of the three phosphorus compounds obtained from spectral deconvolution.

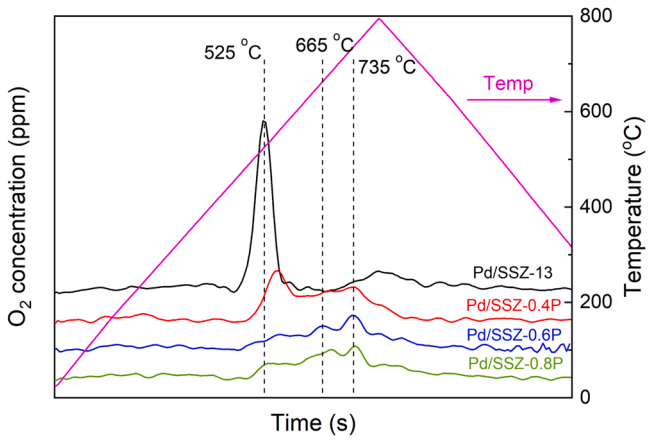

Fig. 6. O_2-TPD profiles of P-poisoned and non-poisoned Pd/SSZ-13.

Table 2
Amounts of O_2 desorption obtained from O_2-TPD profiles of samples of P-poisoned and non-poisoned Pd/SSZ.

Samples	Pd/SSZ	0.4P	0.6P	0.8P
O_2 (μmol)	0.96	0.81	0.51	0.55

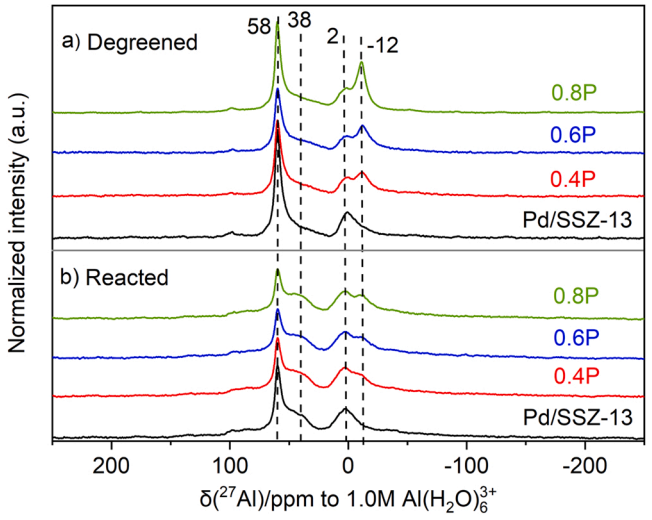

Fig. 7. ^{27}Al NMR of P-poisoned and non-poisoned Pd/SSZ-13: a) degreened and b) reacted. All spectra were normalised according to the weight of the samples.

shown) and no release of oxygen was detected. The amount of O_2 desorption was evaluated by integrating the desorption curves up to 800 ℃; the results are displayed in Table 2. It was clear that increasing the content of phosphorus resulted in less oxygen being released compared with the non-poisoned sample, and that the desorbed quantities reached low values for the highest concentrations of phosphorus (Table 2). The reduction in the amount of oxygen released can be due to the formation of palladium phosphates (phosphates were observed in XPS analysis), with the consequence that less Pd is available for oxygen adsorption/desorption. It is also possible that some of the Pd clusters are blocked physically by the P_2O_5 that was formed, which was also found in the XPS analysis (Figs. 4 and 5).

NMR spectroscopy of ^{27}Al was conducted for both non-poisoned and poisoned Pd/SSZ-13 (i.e. degreened and reacted), the results of which are shown in Fig. 7. Two main chemical shift signals (δ) at 58 and 2 ppm can be observed clearly in the ^{27}Al spectra of all samples (Fig. 7a); these are assigned to tetrahedrally coordinated Al (AlO_4) [48] and octahedral

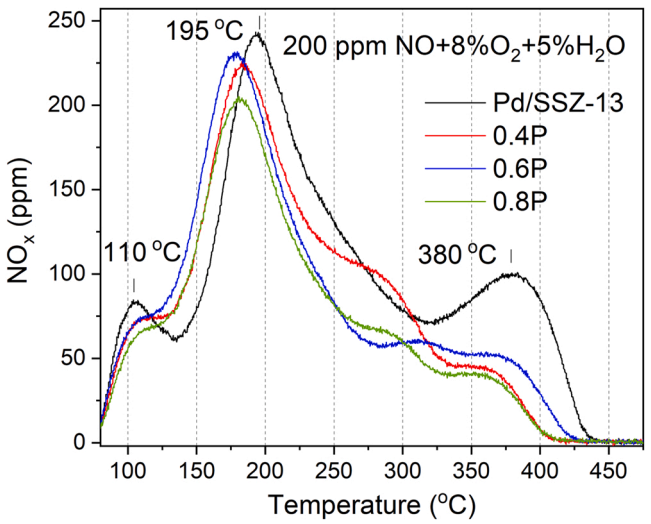

Fig. 8. NO-TPD desorption profiles of non- poisoned and poisoned Pd/SSZ-13.

Table 3
NO_x storage capacity (NO_x/Pd) obtained from the NO-TPD experiments for P-poisoned and non-poisoned Pd/SSZ-13.

Samples	NO_x/Pd Ratio			
	S1 (83–135 ℃)	*S2 (137–319 ℃)*	*S3 (320–438 ℃)*	*Total*
Pd/SSZ	0.08	0.44	0.16	0.68
0.4P	0.06	0.44	0.06	0.56
0.6P	0.05	0.43	0.06	0.54
0.8P	0.04	0.39	0.04	0.47

Al (AlO_6) [49], respectively. The main ^{27}Al signals (58 and 2 ppm) decreased slightly when the P-content was increased, thereby indicating some degree of dealumination of the zeolite lattice. According to the literature, the signal detected around $\delta - 12$ shows the formation of amorphous Al-O-P-species after poisoning [50,51]. This was suggested earlier in the XRD analysis of the shifts observed in some framework-related peaks as well as in SEM-EDX mapping, where the line scan profile showed an overlap of P and Al. The signals detected from the reacted samples (Fig. 7b) resemble the degreened samples (Fig. 7a), indicating that the reaction did not influence the framework. However, a new signal around 38 ppm was detected from the reacted samples that was assigned to pentahedral Al [49,52]. These latter Al species have three bonds or less with the framework in which the coordination sphere of Al is filled by H_2O molecules [53], which most probably originates from exposure to water vapour in the flow reactor. Moreover, the amount of amorphous Al-O-P-species at $\delta - 12$ present in the reacted sample has decreased, supporting the XPS results, i.e. that some of the P_2O_5 that interacts with the zeolite has transformed into PO_3^-.

3.2. NO temperature programmed desorption experiments

NO-TPD experiments were conducted to investigate the effect of phosphorus on passive NO_x adsorption and desorption for different concentrations of phosphorus loading on Pd/SSZ-13. The adsorbents were exposed to 200 ppm NO, 8% O_2 and 5% H_2O at 80 ℃ for 2 h, followed by flushing with 8% O_2, 5% H_2O and Ar for 30 min. Finally, the temperature was increased, at a rate of 20 ℃/min, in the same gas mixture until it reached 550 ℃ for the desorption step; Fig. 8a illustrates the desorption profiles of both poisoned and non-poisoned samples. An obvious deactivation was observed for the phosphorus poisoning of Pd/SSZ-13; compared with the degreened sample, integration of the desorbed NO_x resulted in deactivation at about 17%, 20% and 31% for 0.4P,

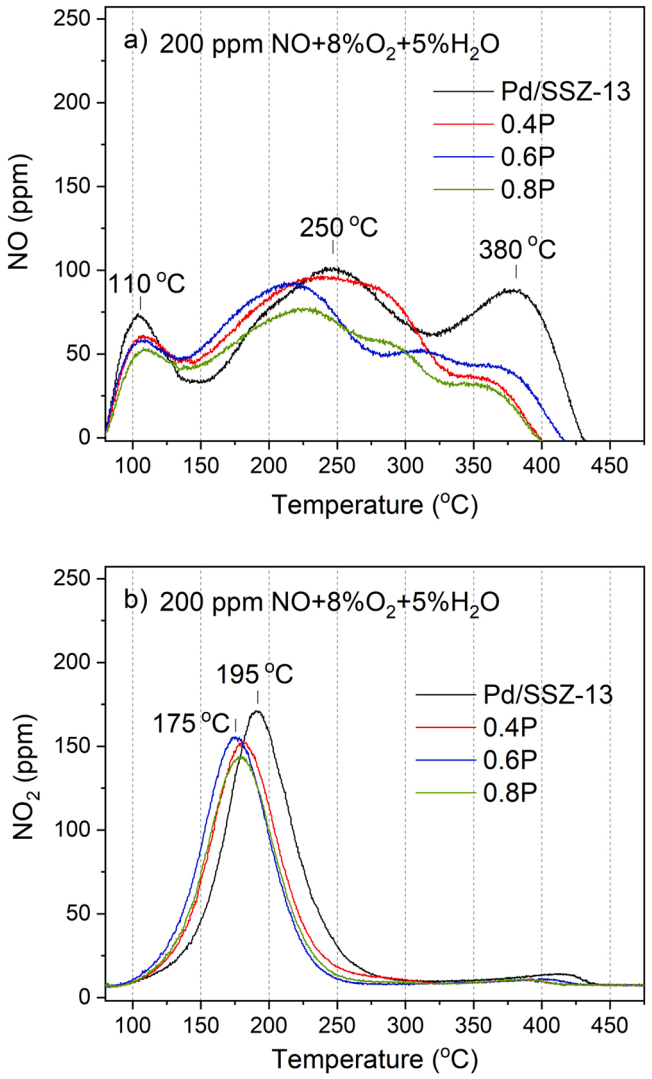

Fig. 9. Desorption profiles of the non- poisoned and P-poisoned Pd/SSZ-13. a) NO profiles and b) NO_2 profiles.

0.6P and 0.8P, respectively. This deactivation was also observed on the adsorption curves, following the trend of the phosphorus content (Fig. S2, Supplementary material).

All the measured NO_x/Pd ratios in Table 3 were lower than 1, suggesting that not all the Pd active sites were available. This can be due to H_2O blockage, but also likely due to formation of PdO clusters/particles formed via the impregnation method. The formation of Pd clusters was confirmed by TEM images as well (Fig. 2). The formed clusters can adsorb NO_x to a lower extent owing to a limited number of exposed Pd surface sites [17,22,54,55].

The NO_x desorption profile revealed three main desorption peaks for Pd/SSZ-13. These were centred around 110, 195 and 380 °C, and could be attributed to three different Pd sites. The profiles of NO and NO_2 during desorption are illustrated in Fig. 9 to provide a better understanding of the desorption mechanism. The temperatures detected for the release of NO were 110 °C, 230–250 °C and 380 °C, and around 185 °C for NO_2. Different studies have reported that the main adsorption sites in Pd zeolite adsorbents are the ion-exchanged Pd cation sites in the zeolite framework [14,17]. These Pd species can bond with either two Al to form $Z^-Pd^{2+}Z^-$ or just one Al and balance the charge with an OH group to form $Z^-[Pd(II)OH)]^+$. At 80 °C, NO_x can be adsorbed at these three sites ($Z^-Pd^{2+}Z^-$, $Z^-[Pd(II)OH)]^+$, PdO) via different reaction mechanisms and will be desorbed at various temperatures in the form of NO or NO_2. DRIFT spectroscopy detected multiple bands in the area 1800–1880 cm^{-1}, which can be attributed to adsorption of NO on $Z^-Pd^{2+}Z^-$ and $Z^-[Pd(II)OH)]^+$sites (Section 3.3). The low temperature desorption peak was mostly associated with NO. With the limited numbers of PdO species, NO desorption at low temperatures (~110 °C) can be due to the decomposition of palladium nitrates ($Pd(II)NO_3$) forming PdO (R1) or other reactions related to the Pd clusters. Formation of Pd nitrates was confirmed by DRIFTS analysis in Section 3.3. Our previous study [22] found that the release of NO at 250 °C from Pd/SSZ-13 was related to NO desorption from $Z^-Pd^{2+}Z^-$ sites (R2), which is assumed to be the case in the present study for NO desorption around 195 °C. DRIFTS analysis also showed a large amount of linear nitrosyl species were formed during NO adsorption (Section 3.3). In other studies, it was reported that $Z^-[Pd(II)OH)]^+$ sites can be reduced by adsorbed NO and form stable bonds that require higher temperatures to release NO compared with other ion exchanged Pd sites [22,56,57]. Thus, the NO release around 380 °C was assigned to the reduced $Z^-[Pd(II)OH)]^+$sites (R3).

$$Pd(II)O + NO + 1.5O_2 \quad \rightleftharpoons \quad Pd(NO_3)_2 \tag{R1}$$

$$Z^-Pd^{2+}Z^- + NO \rightleftharpoons Z^-Pd(II)Z - NO \tag{R2}$$

$$Z^-[Pd(II)OH)]^+ + NO \quad \rightleftharpoons \quad Z^-[Pd(II)OH)]^+ - NO \tag{R3}$$

The middle NO_x desorption peak (175–195 °C) was mostly related to NO_2 around 185 °C. According to the step-test that was conducted in an empty reactor tube (Fig. S3, Supplementary material), very small quantities of NO_2 (~ 3.5 ppm) were present during the adsorption step in the inlet gas feed. Thus, there is a high possibility of NO_2 adsorption at Pd^{2+} sites that can be desorbed at lower temperatures (~195 °C). In addition, NO_2 had a small desorption peak at higher temperatures of around 400 °C that was most probably related to the oxidation of NO to NO_2 in presence of oxygen catalysed by PdO_x clusters [3,55]. We have earlier observed a continuous NO oxidation at higher temperature over Pd/SSZ-13 [22], which supports this finding.

Table 3 presents the NO_x/Pd ratio of the P-poisoned and degreened Pd/SSZ-13 for the three desorption temperature ranges, namely S1: 83–135 °C, S2: 137–319 °C and S3: 320–438 °C: a clear deactivation of the Pd/SSZ-13 can be seen with increasing phosphorus content. This is consistent with the findings of other studies of the phosphorous poisoning of Cu/SSZ-13 used for NH_3-SCR [29,31,42]. A more severe decrease in NO_x desorption at higher temperatures was observed (Table 3) that is associated with NO species with stronger bonds formed on the $Z^-[Pd(II)OH)]^+$ [22,58,59]. The NO_2 profile in Fig. 9b displayed deactivation in both desorption areas around 200 °C and 400 °C in the P-poisoned samples. Lower NO_2 release at high temperatures was attributed to the presence of less available PdO_x nanoparticles in the poisoned samples; this was also observed in the O_2-TPD profiles of these adsorbents, where less released O_2 was detected. In addition, DRIFTS analysis (Section 3.3) showed that the nitrates had an obvious reduction in intensity after P-poisoning, which can explain the lower release of NO_2 at 200 °C after poisoning. Moreover, a temperature shift of about 10 °C was observed in the NO_2 release of P-poisoned samples (Fig. 9b) towards lower values, indicating that phosphorus caused changes to the binding strength on $[Pd(OH)]^+$. Furthermore, it was observed that the NO desorption peak around 380 °C decreased drastically and, for higher concentrations of phosphorus (0.6P and 0.8P), a small peak between 300 and 320 °C appeared.

As mentioned previously, all the samples had been subjected to 5 cycles and the reacted samples were studied after the fifth step, which had the same conditions as the first cycle (200 ppm NO, 8% O_2 and 5% H_2O). It was observed that the Pd/SSZ-13 was still very active after the 5 varying conditional cycles, where the total NO_x release was the same (see Fig. 10). However, the stability increased somewhat for the strongest bonded NO_x after repeated experiments. These results suggest that

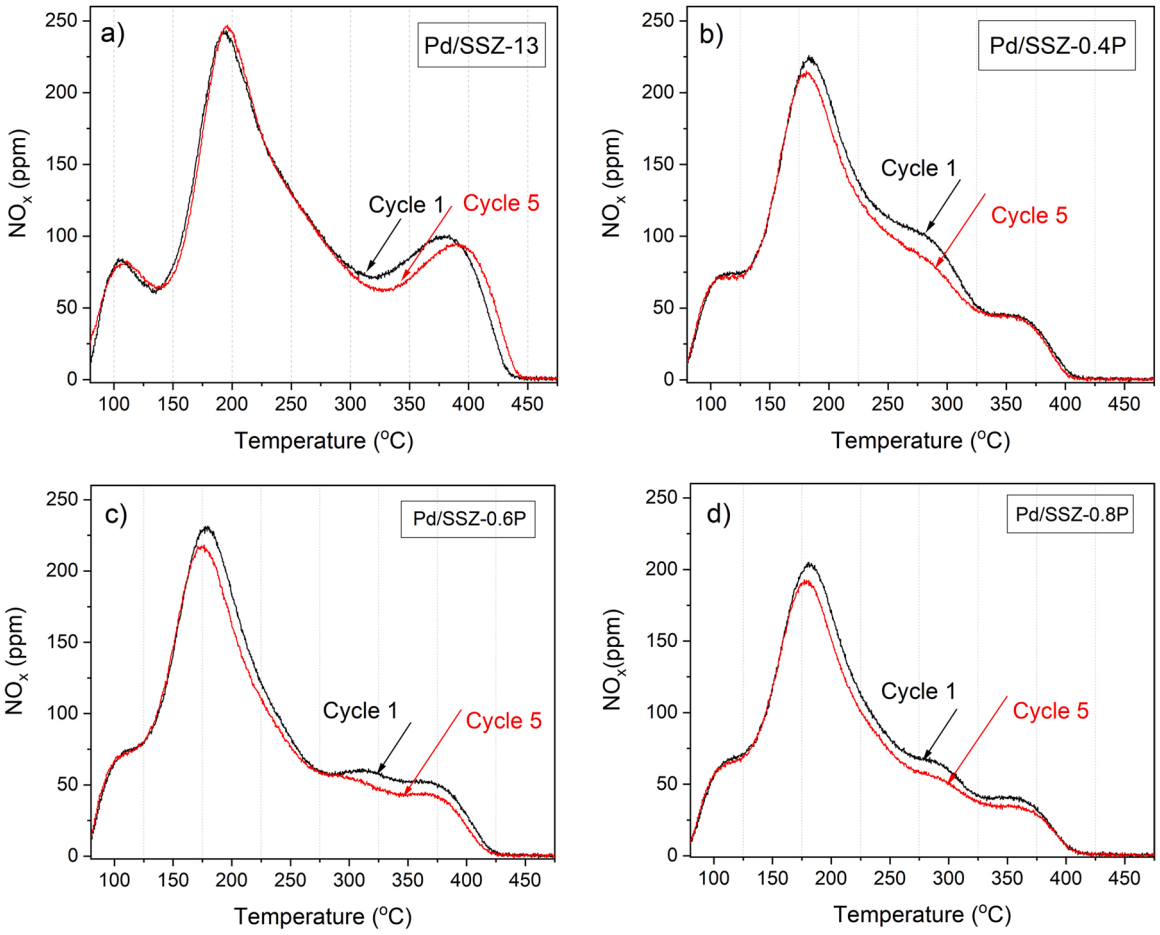

Fig. 10. NO_x concentrations measured in the TPD experiments with 8% O_2, 5% H_2O and 200 ppm NO for the first and fifth cycles. a) Pd/SSZ-13, b) Pd/SSZ-0.4P, c) Pd/SSZ-0.6P and d) Pd/SSZ-0.8P.

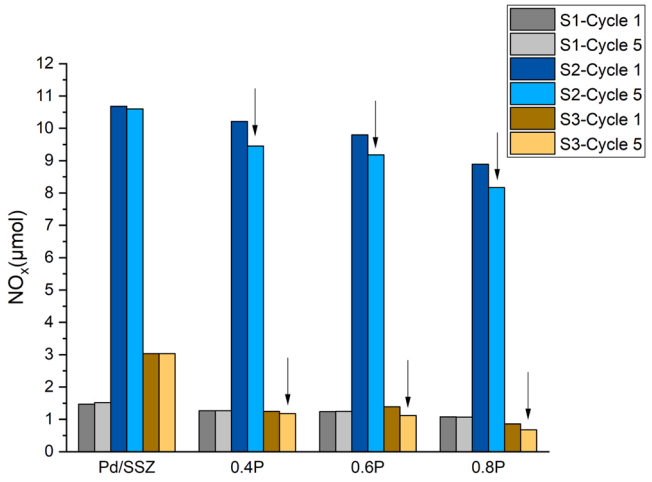

Fig. 11. Amounts of NO_x released at the S1, S2 and S3 sites in Cycle 1 and Cycle 5 for Pd/SSZ-13, 0.4P, 0.6P and 0.8P. S1: 83–135 °C, S2: 137–319 °C and S3: 320–438 °C.

the binding strength of NO at reduced $Z^{-}[Pd(II)OH)]^{+}$ sites was increased after repeated experiments. In the case of the P-poisoned samples, on the other hand, the total capacity decreased after 5 cycles by 6%, 7% and 9% for the 0.4, 0.6 and 0.8 samples, respectively (Fig. 10). The effect of P-poisoning was therefore greater after repeated experiments and the increased deactivation after repeated cycles was more severe when larger quantities of phosphorus were used.

Fig. 11 shows the amount of NO_x released (μmol) from the different desorption sites (S1: 83–135 °C, S2: 137–319 °C and S3: 320–438 °C) in Cycles 1 and 5 for the non-poisoned and poisoned samples. After multiple cycles, the greatest changes occurred in NO_x releases at higher temperatures (S2 and S3), which are related to NO_x desorption from $Z^{-}[Pd(II)OH)]^{+}$ and $Z^{-}Pd^{2+}Z^{-}$ adsorption sites. XPS analysis of P-poisoned adsorbents showed the formation of greater quantities of PO_3^{-} and lesser quantities of P_2O_5 post reaction. Some of the P_2O_5 that caused physical deactivation was therefore transformed into PO_3^{-} during the cycling experiments, which is responsible for chemical deactivation. The chemical deactivation of the Pd sites was irreversible during our reaction conditions; the increased formation of PO_3^{-} can explain why the storage and release of NO_x were reduced after repeated cycles of P-poisoned samples.

3.3. *In-situ DRIFT spectroscopy*

In situ NO and NO+CO DRIFT spectroscopy was conducted to observe the effect of phosphorus on the adsorption of NO and CO. The adsorbents were exposed initially to 200 ppm NO, 1% H_2O and 8% O_2 in Ar at 80 °C for 15 min; after the desorption step at 550 °C, 400 ppm CO was added during the next adsorption step at 80 °C for 15 min to provide a better understanding of both the NO and CO adsorption sites (Fig. 12). Under NO-DRIFTS analysis it was observed that Pd nitrate species (1317–1523 cm^{-1}) [60] were reduced in the P-poisoned samples (Fig. S4 Supplementary material). This can explain the decrease seen in the NO_2 desorption peak at 200 °C with the presence of phosphorus that

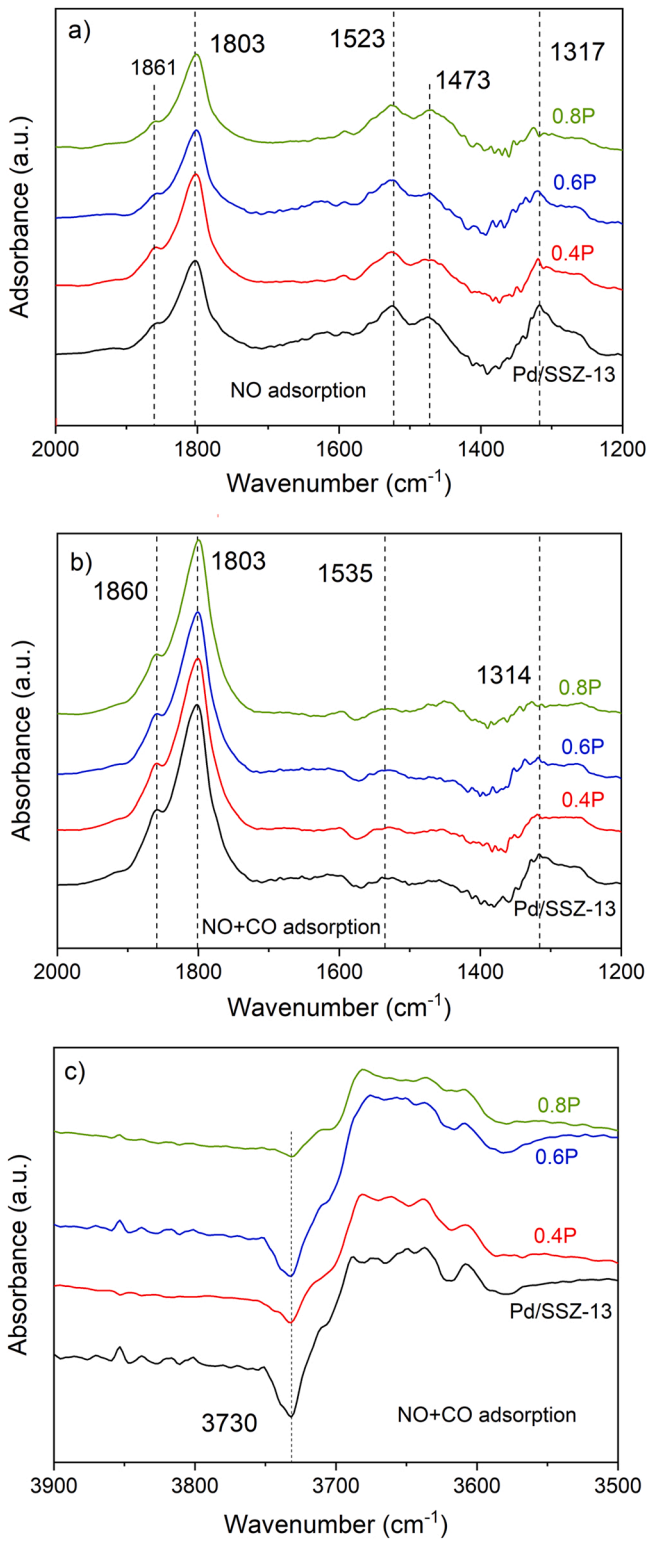

Fig. 12. DRIFT spectra obtained from a) 200 ppm NO and b) 200 ppm NO and 400 ppm CO between 1200 and 2000 cm^{-1} at 80 °C; and c) 200 ppm NO and 400 ppm CO between 3500 and 3900 cm^{-1} at 80 °C. 1% H_2O and 8% O_2 were present in all experiments.

reduced the possibility of nitrates forming (Section 3.2) and that fewer PdO_x species were available, as seen during the O_2 TPD experiments (Fig. 6 and Table 2). Peaks around 1861 and 1803 cm^{-1} in NO-DRIFTS were assigned to linear nitrosyl species, where NO is attached to the cationic Pd^{2+} (Pd^{2+}-NO) [18,61]. However, no reduction in intensity was observed for these peaks after P-poisoning. The nitrate peaks cannot be detected as clearly in the NO + CO adsorption step because $Pd(NO_3)_2$ species cannot be formed easily due to the reduction of PdO species caused by CO [22]. According to the literature other species, such as Pd $(CO)_x$, Pd-NO and Pd-(NO)(CO), can be detected around 2146, 1859 and 1801 cm^{-1}, respectively, appear with the presence of CO [54,62]. In the NO + CO step, the 1860 and 1803 cm^{-1} peaks showed a lower intensity for the P-poisoned samples, which can be due to deactivation of these samples. The band detected around 3730 cm^{-1} was related to $Al^{VI}(OH)Al^{VI}$ bonded to octahedral aluminium [63] and a clear intensity reduction was observed for this peak P-poisoning of the samples, suggesting that the OH groups had been interacting with phosphorus. This concurs with the findings of XPS, XRD and NMR. The XPS results showed the formation of P_2O_5, which can lead to physical deactivation of the support (Figs. 4 and 5). The reaction of the OH groups were also observed for Pd loaded zeolite in other studies as well [31,32]. The XRD pattern showed a shift caused by the interaction of P with the support (Fig. 3) and NMR showed the appearance of a new peak for the Al-O-P species (Fig. 7). It may be concluded that the support material can react with phosphorus and form species such as $AlPO_4$ and/or $Al(PO_3)_3$.

4. Conclusions

The main aim of this study was to investigate the effect of phosphorus poisoning on the activity of Pd/SSZ-13 in a passive NO_x adsorption process. Using an incipient wetness impregnation technique, samples of 1 wt% Pd on SSZ-13 were prepared with three different levels of phosphorus poisoning: 0.4, 0.6 and 0.8 mmol g^{-1}. Comparison of the activity of the P-poisoned and non-poisoned Pd/SSZ-13 showed an obvious deactivation of the adsorbent as the P loading was increased. It was more severe for the release of NO at high temperatures (380 °C) and NO_2 at 185 °C. This was also observed in the DRIFTS analysis, where the intensity of the nitrate peaks reduced after poisoning.

The physical effect of phosphorus was observed distinctly in the reduction of the surface area and pore volume of the Pd/SSZ-13 after P-poisoning. Surface blockage could also possibly be the reason why the P-poisoned samples released less O_2, as shown by the O_2-TPD analysis. A clear overlap of phosphorus on Pd and Al was detected by SEM-EDX mapping: this suggests the interaction of phosphorus with the metal and zeolite framework, which can cause both chemical and physical deactivation in the adsorbent. XPS analysis clearly showed that phosphorus caused both physical and chemical deactivation: the former through the presence of P_2O_5 and the latter through the presence of PO_3^- and PO_4^{3}. Moreover, higher concentrations of phosphorus led to the formation of larger quantities of PO_3^-. We therefore also suggest that a possible reason for the lower release of O_2 from the P-poisoned samples in O_2-TPD was the formation of palladium phosphates, which lead to less oxygen being adsorbed. Both XRD and ^{27}Al-NMR clearly showed the interaction of phosphorus with the zeolite structure, where shifts around $2\theta = 9.6°$, 18° and 25.3° in the XRD spectra were due to the expansion of lattice planes from phosphorus located in the zeolite structure, whilst ^{27}Al-NMR measurements exposed a new peak at around $\delta - 12$ due to the presence of Al-O-P-species after P-poisoning of the adsorbents. This result was consistent with the DRIFT spectroscopy, which revealed a lower intensity of the $Al^{VI}(OH)Al^{VI}$ bonds in the zeolite structure and thereby supports the finding that phosphorus poisons the OH groups.

The activity of the samples also confirmed that phosphorus could cause permanent deactivation of the adsorbent. Moreover, the storage ability of P-poisoned samples declined after multiple cycles. We suggest that this was due to the transformation of P_2O_5 to PO_3^- during multiple cycles, as shown by XPS: P_2O_5 blocks the catalyst and deactivates physically, whereas PO_3^- interacts with the Pd species and deactivates chemically. Thus, some of the phosphorus is transformed and results in further chemical deactivation of the Pd species which, in turn, decreases the functionality of the PNA.

CRediT authorship contribution statement

Rojin Feizie Ilmasani: Conceptualization, Investigation, Formal analysis, Writing – original draft. **Dawei Yao:** Formal analysis, Writing – review & editing. **Phuoc Hoang Ho:** Formal analysis, Writing – review & editing. **Diana Bernin:** Formal analysis, Writing – review & editing. **Derek Creaser:** Conceptualization, Supervision, Writing – review & editing. **Louise Olsson:** Conceptualization, Supervision, Writing – review & editing, Funding acquisition.

Declaration of Competing Interest

The authors declare that they have no known competing financial interests or personal relationships that could have appeared to influence the work reported in this paper.

Acknowledgements

This work was performed at the Chemical Engineering and the Competence Centre for Catalysis at Chalmers University of Technology. Stefan Gustavsson, at CMAL at the Chalmers University of Technology, is thanked for his help with the SEM measurements. The Swedish NMR Center is acknowledged for the spectrometer time we were generously allocated. Funding from the Swedish Research Council (642-2014-5733) is gratefully acknowledged.

Appendix A. Supporting information

Supplementary data associated with this article can be found in the online version at doi:10.1016/j.jece.2022.107608.

References

[1] E.C. Dykes, NOx performance of an LNT+SCR system designed to meet EPA 2010 emissions: results of engine dynamometer emission tests, SAE Int. J. Commer. Veh. 1 (2008) 327–337.
[2] J.E. De Abreu Goes, L. Olsson, M. Berggrund, A. Kristoffersson, L. Gustafson, M. Hicks, Performance studies and correlation between vehicle- and rapid- aged commercial lean NOx trap catalysts, SAE Int. J. Engines 10 (2017) 1613–1626.
[3] A. Wang, K. Xie, A. Kumar, K. Kamasamudram, L. Olsson, Layered Pd/SSZ-13 with Cu/SSZ-13 as PNA – SCR dual-layer monolith catalyst for NOx abatement, Catal. Today (2020).
[4] A.M. Beale, F. Gao, I. Lezcano-Gonzalez, C.H. Peden, J. Szanyi, Recent advances in automotive catalysis for NO x emission control by small-pore microporous materials, Chem. Soc. Rev. 44 (2015) 7371–7405.
[5] P. Forzatti, I. Nova, E. Tronconi, New "Enhanced NH3-SCR" reaction for NOx emission control, Ind. Eng. Chem. Res. 49 (2010) 10386–10391.
[6] O. Mihai, L. Trandafilović, T. Wentworth, F.F. Torres, L. Olsson, The effect of Si/Al ratio for Pd/BEA and Pd/SSZ-13 used as passive NOx adsorbers, Top. Catal. 61 (2018) 2007–2020.
[7] S. Jones, Y. Ji, A. Bueno-Lopez, Y. Song, M. Crocker, CeO2-M2O3 passive NOx adsorbers for cold start applications, Emiss. Control Sci. Technol. 3 (2017) 59–72.
[8] V. Schmeisser, M. Weibel, L. Sebastian Hernando, I. Nova, E. Tronconi, M.P. Ruggeri, Cold start effect phenomena over zeolite scr catalysts for exhaust gas aftertreatment, SAE International, 2013.
[9] S. Ren, S.J. Schmieg, C.K. Koch, G. Qi, W. Li, Investigation of Ag-based low temperature NOx adsorbers, Catal. Today 258 (2015) 378–385.
[10] Y. Ji, S. Bai, M. Crocker, Al 2 O 3-based passive NOx adsorbers for low temperature applications, Appl. Catal. B: Environ. 170 (2015) 283–292.
[11] Y. Ji, D. Xu, S. Bai, U. Graham, M. Crocker, B. Chen, C. Shi, D. Harris, D. Scapens, J. Darab, Pt- and Pd-promoted CeO2–ZrO2 for passive NOx adsorber applications, Ind. Eng. Chem. Res. 56 (2017) 111–125.
[12] S. Tamm, S. Andonova, L. Olsson, Silver as storage compound for NOx at low temperatures, Catal. Lett. 144 (2014) 674–684.
[13] Y. Ryou, J. Lee, H. Lee, C.H. Kim, D.H. Kim, Effect of sulfur aging and regeneration on low temperature NO adsorption over hydrothermally treated Pd/CeO2 and Pd/Ce0. 58Zr0. 42O2 catalysts, Catal. Today 297 (2017) 53–59.
[14] H.-Y. Chen, J.E. Collier, D. Liu, L. Mantarosie, D. Durán-Martín, V. Novák, R. R. Rajaram, D. Thompsett, Low temperature NO storage of zeolite supported Pd for low temperature diesel engine emission control, Catal. Lett. 146 (2016) 1706–1711.
[15] Z. Ma, L. Sheng, X. Wang, W. Yuan, S. Chen, W. Xue, G. Han, Z. Zhang, H. Yang, Y. Lu, Oxide catalysts with ultrastrong resistance to SO2 deactivation for removing nitric oxide at low temperature, Adv. Mater. 31 (2019), 1903719.
[16] A. Porta, T. Pellegrinelli, L. Castoldi, R. Matarrese, S. Morandi, S. Dzwigaj, L. Lietti, Low temperature NO x adsorption study on Pd-promoted zeolites, Top. Catal. 61 (2018) 2021–2034.
[17] Y. Zheng, L. Kovarik, M.H. Engelhard, Y. Wang, Y. Wang, F. Gao, J. Szanyi, Low-temperature Pd/zeolite passive NOx adsorbers: structure, performance, and adsorption chemistry, J. Phys. Chem. C 121 (2017) 15793–15803.
[18] Y. Ryou, J. Lee, S.J. Cho, H. Lee, C.H. Kim, D.H. Kim, Activation of Pd/SSZ-13 catalyst by hydrothermal aging treatment in passive NO adsorption performance at low temperature for cold start application, Appl. Catal. B: Environ. 212 (2017) 140–149.
[19] A. Vu, J. Luo, J. Li, W.S. Epling, Effects of CO on Pd/BEA passive NOx adsorbers, Catal. Lett. 147 (2017) 745–750.
[20] R.P.Z. Yuntao Gu, Yu-Ren Chen, William S. Epling, Investigation of an irreversible NOx storage degradation mode on a Pd/BEA passive NOx adsorber, Appl. Catal. B: Environ. 258 (2019), 118032.
[21] J.R. Theis, J.A. Ura, Assessment of zeolite-based low temperature NOx adsorbers: effect of reductants during multiple sequential cold starts, Catal. Today (2020).
[22] D. Yao, R. Feizie Ilmasani, J.C. Wurzenberger, T. Glatz, J. Han, A. Wang, D. Creaser, L. Olsson, Kinetic modeling of CO assisted passive NOx adsorption on Pd/SSZ-13, Chem. Eng. J. 428 (2022), 132459.
[23] R.F. Ilmasnai, Chemical Poisoning of Lean NOx Traps Used for Cleaning Emissions from Vehicles, Sweden, Göteborg, 2017.
[24] S.J. Eaton, B.G. Bunting, T.J. Toops, The Roles of Phosphorus and Soot on the Deactivation of Diesel Oxidation Catalysts, SAE International, 2009.
[25] A. Väliheikki, M. Kärkkäinen, M. Honkanen, O. Heikkinen, T. Kolli, K. Kallinen, M. Huuhtanen, M. Vippola, J. Lahtinen, R.L. Keiski, Deactivation of Pt/SiO2-ZrO2 diesel oxidation catalysts by sulphur, phosphorus and their combinations, Appl. Catal. B: Environ. 218 (2017) 409–419.
[26] K. Xie, A. Wang, J. Woo, A. Kumar, K. Kamasamudram, L. Olsson, Deactivation of Cu-SSZ-13 SCR catalysts by vapor-phase phosphorus exposure, Appl. Catal. B: Environ. 256 (2019), 117815.
[27] P. Anguita, J.M. García-Vargas, F. Gaillard, E. Iojoiu, S. Gil, A. Giroir-Fendler, Effect of Na, K, Ca and P-impurities on diesel oxidation catalysts (DOCs), Chem. Eng. J. 352 (2018) 333–342.
[28] H. Zhao, Y. Zhao, M. Liu, X. Li, Y. Ma, X. Yong, H. Chen, Y. Li, Phosphorus modification to improve the hydrothermal stability of a Cu-SSZ-13 catalyst for selective reduction of NOx with NH3, Appl. Catal. B: Environ. 252 (2019) 230–239.
[29] A. Wang, J. Wang, S. Sheti, S. Dahlin, J. Han, J. Woo, K. Xie, L.J. Pettersson, L. Olsson, A deactivation mechanism study of phosphorus-poisoned diesel oxidation catalysts: model and supplier catalysts, Catal. Sci. Technol. 10 (2020) 5602–5617.
[30] M.J. Rokosz, A.E. Chen, C.K. Lowe-Ma, A.V. Kucherov, D. Benson, M.C. Paputa Peck, R.W. McCabe, Characterization of phosphorus-poisoned automotive exhaust catalysts, Appl. Catal. B: Environ. 33 (2001) 205–215.
[31] K. Xie, J. Woo, D. Bernin, A. Kumar, K. Kamasamudram, L. Olsson, Insights into hydrothermal aging of phosphorus-poisoned Cu-SSZ-13 for NH3-SCR, Appl. Catal. B: Environ. 241 (2019) 205–216.
[32] D. Chen, H. Lei, W. Xiong, Y. Li, X. Ji, J.-Y. Yang, B. Peng, M. Fu, P. Chen, D. Ye, Unravelling phosphorus-induced deactivation of Pd-SSZ-13 for passive NOx adsorption and CO oxidation, ACS Catal. 11 (2021) 13891–13901.
[33] R.F. Ilmasani, J. Woo, D. Creaser, L. Olsson, Influencing the NOx stability by metal oxide addition to Pd/BEA for passive NOx adsorbers, Ind. Eng. Chem. Res. 59 (2020) 9830–9840.
[34] A. Wang, K. Xie, D. Bernin, A. Kumar, K. Kamasamudram, L. Olsson, Deactivation mechanism of Cu active sites in Cu/SSZ-13—phosphorus poisoning and the effect of hydrothermal aging, Appl. Catal. B: Environ. 269 (2020), 118781.
[35] L. Xie, F. Liu, X. Shi, F.-S. Xiao, H. He, Effects of post-treatment method and Na co-cation on the hydrothermal stability of Cu–SSZ-13 catalyst for the selective catalytic reduction of NOx with NH3, Appl. Catal. B: Environ. 179 (2015) 206–212.
[36] Z. Zhao, R. Yu, R. Zhao, C. Shi, H. Gies, F.-S. Xiao, D. De Vos, T. Yokoi, X. Bao, U. Kolb, M. Feyen, R. McGuire, S. Maurer, A. Moini, U. Müller, W. Zhang, Cu-exchanged Al-rich SSZ-13 zeolite from organotemplate-free synthesis as NH3-SCR catalyst: effects of Na+ ions on the activity and hydrothermal stability, Appl. Catal. B: Environ. 217 (2017) 421–428.
[37] K. Xie, K. Leistner, K. Wijayanti, A. Kumar, K. Kamasamudram, L. Olsson, Influence of phosphorus on Cu-SSZ-13 for selective catalytic reduction of NOx by ammonia, Catal. Today 297 (2017) 46–52.
[38] T. Arunagiri, T.D. Golden, O. Chyan, Study of palladium metal particle deposition on the conductive diamond surface by XRD, XPS and electrochemistry, Mater. Chem. Phys. 92 (2005) 152–158.
[39] A.K. Datye, J. Bravo, T.R. Nelson, P. Atanasova, M. Lyubovsky, L. Pfefferle, Catalyst microstructure and methane oxidation reactivity during the Pd↔PdO transformation on alumina supports, Appl. Catal. A: Gen. 198 (2000) 179–196.
[40] H.E. van der Bij, B.M. Weckhuysen, Phosphorus promotion and poisoning in zeolite-based materials: synthesis, characterisation and catalysis, Chem. Soc. Rev. 44 (2015) 7406–7428.
[41] D. Briggs, Handbook of X-ray Photoelectron Spectroscopy C. D. Wanger, W. M. Riggs, L. E. Davis, J. F. Moulder and G. E.Muilenberg Perkin-Elmer Corp., Physical Electronics Division, Eden Prairie, Minnesota, USA, 1979. 190. Surf. Interface Anal. (1981) 3, v.
[42] S. Andonova, E. Vovk, J. Sjöblom, E. Ozensoy, L. Olsson, Chemical deactivation by phosphorous under lean hydrothermal conditions over Cu/BEA NH3-SCR catalysts, Appl. Catal. B: Environ. 147 (2014) 251–263.
[43] S. Shwan, J. Jansson, L. Olsson, M. Skoglundh, Chemical deactivation of Fe-BEA as NH3-SCR catalyst—effect of phosphorous, Appl. Catal. B: Environ. 147 (2014) 111–123.

[44] L.L. Hegedus, K. Baron, Phosphorus accumulation in automotive catalysts, J. Catal. 54 (1978) 115–119.
[45] V. Kröger, M. Hietikko, D. Angove, D. French, U. Lassi, A. Suopanki, R. Laitinen, R. L. Keiski, Effect of phosphorus poisoning on catalytic activity of diesel exhaust gas catalyst components containing oxide and Pt, Top. Catal. 42 (2007) 409–413.
[46] Y. Lou, J. Ma, W. Hu, Q. Dai, L. Wang, W. Zhan, Y. Guo, X.-M. Cao, Y. Guo, P. Hu, G. Lu, Low-temperature methane combustion over Pd/H-ZSM-5: active Pd sites with specific electronic properties modulated by acidic sites of H-ZSM-5, ACS Catal. 6 (2016) 8127–8139.
[47] L.M.T. Simplício, S.T. Brandão, E.A. Sales, L. Lietti, F. Bozon-Verduraz, Methane combustion over PdO-alumina catalysts: the effect of palladium precursors, Appl. Catal. B: Environ. 63 (2006) 9–14.
[48] J.M. Jeong, J.H. Park, J.H. Baek, R.H. Hwang, S.G. Jeon, K.B. Yi, Effect of acid treatment of Fe-BEA zeolite on catalytic N2O conversion, Korean J. Chem. Eng. 34 (2017) 81–86.
[49] Y. Ryou, J. Lee, H. Lee, C.H. Kim, D.H. Kim, Effect of various activation conditions on the low temperature NO adsorption performance of Pd/SSZ-13 passive NOx adsorber, Catal. Today 320 (2019) 175–180.
[50] M. Bernhard, W. Reschetilowski, S. Paasch, Spectroscopic study of phosphorus modified H-ZSM-5, Microporous Mesoporous Mater 142 (2011) 178–183.
[51] D. Müller, I. Grunze, E. Hallas, G. Ladwig, Hochfeld-27Al-NMR-Untersuchungen zur Aluminiumkoordination in Kristallinen Aluminiumphosphaten, Z. Anorg. Allg. Chem. 500 (1983) 80–88.
[52] F. Gao, Y. Wang, N.M. Washton, M. Kollár, J. Szanyi, C.H.F. Peden, Effects of alkali and alkaline earth cocations on the activity and hydrothermal stability of Cu/SSZ-13 NH3-SCR catalysts, ACS Catal. 5 (2015) 6780–6791.
[53] S. Prodinger, M.A. Derewinski, Y. Wang, N.M. Washton, E.D. Walter, J. Szanyi, F. Gao, Y. Wang, C.H.F. Peden, Sub-micron Cu/SSZ-13: synthesis and application as selective catalytic reduction (SCR) catalysts, Appl. Catal. B: Environ. 201 (2017) 461–469.
[54] K. Khivantsev, F. Gao, L. Kovarik, Y. Wang, J. Szanyi, Molecular level understanding of how oxygen and carbon monoxide improve NOx storage in palladium/SSZ-13 passive NOx adsorbers: the role of NO+ and Pd(II)(CO)(NO) species, J. Phys. Chem. C 122 (2018) 10820–10827.
[55] A. Wang, K. Lindgren, M. Di, D. Bernin, P.-A. Carlsson, M. Thuvander, L. Olsson, Insight into hydrothermal aging effect on Pd sites over Pd/LTA and Pd/SSZ-13 as PNA and CO oxidation monolith catalysts, Appl. Catal. B: Environ. 278 (2020), 119315.
[56] M. Ambast, K. Karinshak, B.M.M. Rahman, L.C. Grabow, M.P. Harold, Passive NOx adsorption on Pd/H-ZSM-5: experiments and modeling, Appl. Catal. B: Environ. (2020), 118802.
[57] K. Mandal, Y. Gu, K.S. Westendorff, S. Li, J.A. Pihl, L.C. Grabow, W.S. Epling, C. Paolucci, Condition-dependent Pd speciation and NO adsorption in Pd/Zeolites, ACS Catal. 10 (2020) 12801–12818.
[58] B. Lin, A. Wang, Y. Guo, Y. Ding, Y. Guo, L. Wang, W. Zhan, F. Gao, Ambient temperature NO adsorber derived from pyrolysis of Co-MOF(ZIF-67), ACS Omega 4 (2019) 9542–9551.
[59] A. Wang, Y. Guo, F. Gao, C.H.F. Peden, Ambient-temperature NO oxidation over amorphous CrOx-ZrO2 mixed oxide catalysts: significant promoting effect of ZrO2, Appl. Catal. B: Environ. 202 (2017) 706–714.
[60] T. Baidya, P. Bera, B. Mukri, S. Parida, O. Kröcher, M. Elsener, M.S. Hegde, DRIFTS studies on CO and NO adsorption and NO plus CO reaction over Pd2+-substituted CeO2 and Ce0.75Sn0.25O2 catalysts, J. Catal. 303 (2013) 117–129.
[61] K. Khivantsev, N.R. Jaegers, L. Kovarik, J.C. Hanson, F. Tao, Y. Tang, X. Zhang, I. Z. Koleva, H.A. Aleksandrov, G.N. Vayssilov, Y. Wang, F. Gao, J. Szanyi, Achieving atomic dispersion of highly loaded transition metals in small-pore zeolite SSZ-13: high-capacity and high-efficiency low-temperature CO and passive NOx adsorbers, Angew. Chem. Int. Ed. 57 (2018) 16672–16677.
[62] K. Chakarova, E. Ivanova, K. Hadjiivanov, D. Klissurski, H. Knözinger, Co-ordination chemistry of palladium cations in Pd-H-ZSM-5 as revealed by FTIR spectra of adsorbed and co-adsorbed probe molecules (CO and NO), Phys. Chem. Chem. Phys. 006 (2004) 3702–3709.
[63] O.B. Belskaya, I.G. Danilova, M.O. Kazakov, R.M. Mironenko, A.V. Lavrenov, V. A. Likholobov, FTIR spectroscopy of adsorbed probe molecules for analyzing the surface properties of supported Pt (Pd) catalysts, in: P.T. Theophile (Ed.), Infrared Spectroscopy in Materials Science, Engineering and Technology, InTech, 2012.